Ionics (2008) 14:501–507
DOI 10.1007/s11581-008-0207-2

ORIGINAL PAPER

Structural and electrochemical investigation of $LiNi_{0.8}Co_{0.2-x}M_xO_2$ (M=Al, Al+Mg, Al+Mg+Fe) synthesized by solid-state method

V. Sethuprakhash · W. J. Basirun

Received: 11 December 2007 / Accepted: 18 January 2008 / Published online: 4 March 2008

Abstract Lithium nickel cobalt oxide materials doped with Al, Mg, and Fe were synthesized by solid-state reaction at 800 °C for 18 h to study the effects of adding transition and nontransition metals to the structure. Crystalline compounds were obtained as revealed by powder X-ray diffraction (XRD). Energy dispersive analysis of X-rays (EDAX) was used to determine the elemental ratio of all the samples. Impedance measurements showed that all samples have decreasing conductivities at higher temperatures and gave negative activation energies. The addition of nontransition metals actually decreased the conductivities of the materials.

Keywords Cathode materials · Lithium nickel oxide · Lithium nickel cobalt oxide

Introduction

Lithium nickelate [1–3] is becoming one of the most promising positive electrode materials for lithium-ion batteries. Research in cathode materials for rechargeable lithium batteries has a great deal of interest on the layered $LiNiO_2$ and $LiCoO_2$ materials in recent years [4–6]. Doped $LiNiO_2$ may possess better electrochemical properties than $LiNiO_2$ or $LiCoO_2$. Single-phase $LiNi_{0.8}C_{0.2}O_2$ material was prepared by Saadoune and Delmas at 800 °C [7]. Charge–discharge cycling of $LiNi_{1-y}Al_yO_2$ as positive electrode material in lithium cells has shown that aluminum substitution suppresses all the phase transitions observed for the $LiNiO_2$ system [10].

According to Fujita et al. [8] $LiNi_{0.85}Co_{0.15}O_2$ can be prepared at temperatures as low as 400 °C. Recently, Madhavi et al. [9] have examined the cathodic behavior of aluminum substituted phases, $LiNi_{0.7}Co_{0.3-z}Al_zO_2$ ($0 \leq z \leq 0.20$) and established that the composition with z=0.05 showed the optimum behavior in which it retains 70% of the initial discharge capacity at the end of 100 charge–discharge cycles [9]. Therefore, the combined Co and Al substitution for nickel appears very promising because it allows the positive effect of cobalt with improvements of the lamellar character of the structure and the electrochemical properties [10].

A decrease in the nickel ions in the interslab space was observed by cobalt substitution, leading to an improvement of the electrochemical properties [11–15]. Previous studies done on the $LiNi_{1-y-z}Co_yAl_zO_2$ materials confirm the great interest in their electrochemical properties and thermal stabilities of these materials [16–18]. In this study, the structural characterization and electrochemical properties of these four materials are presented: $LiNi_{0.8}Co_{0.2}O_2$, $LiNi_{0.8}Co_{0.1}Al_{0.1}O_2$, $LiNi_{0.8}Co_{0.1}Al_{0.05}Mg_{0.05}O_2$, and $LiNi_{0.8}Co_{0.1}Al_{0.05}Mg_{0.025}Fe_{0.025}O_2$.

Experimental

The single-phase cathode $LiNi_{0.8}Co_{0.2-x}M_xO_2$ (M=Al, Al+Mg, Al+Mg+Fe), which are (C1) $LiNi_{0.8}Co_{0.2}O_2$, (C2) $LiNi_{0.8}Co_{0.1}Al_{0.1}O_2$, (C3) $LiNi_{0.8}Co_{0.1}Al_{0.05}Mg_{0.05}O_2$, and (C4) $LiNi_{0.8}Co_{0.1}Al_{0.05}Mg_{0.025}Fe_{0.025}O_2$, were prepared using the solid-state reaction method. A stoichiometric amount of $LiNO_3$ (formula weight=68.94), $Ni(NO_3)_2.6H_2O$ (formula weight=290.81), $Co(NO_3)_2 \cdot 6H_2O$ (formula

V. Sethuprakhash · W. J. Basirun (✉)
Department of Chemistry, University of Malaya,
50603 Kuala Lumpur, Malaysia
e-mail: jeff@um.edu.my

weight=291.03), $Al(NO_3)_3{\cdot}9H_2O$ (formula weight= 375.14), $Mg(NO_3)_2{\cdot}6H_2O$ (formula weight=256.41), and $Fe(NO_3)_3{\cdot}9H_2O$ (formula weight=404), from Aldrich Chemicals (99.5% assay), were mixed in a porcelain crucible and calcined in a furnace at 800 °C for 18 h. The cathode materials were then left to cool to room temperature and were ground with a mortar and pestle until it becomes a fine powder.

To investigate the crystal structure, the powder obtained was analyzed by performing the X-ray diffraction (XRD) method using PHILIPS PW 1840 powder diffractometer instrument. The scan data were collected in the 2θ range of $10<2\theta<180°$. The ratios of all elements of the materials were identified by energy dispersive analysis of X-rays (EDAX), which was attached to the scanning electron microscopy (SEM) PHILIPS MODEL 515 SEM instrument.

The composite electrodes were prepared by mixing the cathode material $LiNi_{0.8}Co_{0.2-x}M_xO_2$ (M=Al, Al+Mg, Al+Mg+Fe) powder, suitable binding agent, and activated carbon in acetone. After a homogeneous blend was obtained, the mixture was cast onto a glass surface to form a film which was attached to an aluminum mesh current collector. Finally, the materials were cut into round shapes with diameters of 1 cm and used as the cathode. Mesocarbon microbead (MCMB) was used as the anode and 1 M $LiPF_6$ salt in equal volumes of ethylene carbonate (EC), dimethylene carbonate (DMC), and propylene carbonate (PC) was used as the electrolyte.

Impedance spectroscopy was done for all the materials at different temperatures by Hioki Instrument. Cyclic voltammetry was performed using AutoLab PGSTAT 30 Potentiostat–Galvanostat instrument using lithium metal as the counter electrode and the reference electrode in an electrochemical cell assembled in a dry box in an argon gas environment.

Result and discussion

Materials structure characterization

From the EDAX results shown in Table 1, it can be seen that the amount of atomic ratios of all elements in the cathodic material are agreeable with the amount of starting materials.

Figures 1, 2, 3, and 4 shows the XRD patterns of (C1) $LiNi_{0.8}Co_{0.2}O_2$, (C2) $LiNi_{0.8}Co_{0.1}Al_{0.1}O_2$, (C3) $LiNi_{0.8}Co_{0.1}Al_{0.05}Mg_{0.05}O_2$, and (C4) $LiNi_{0.8}Co_{0.1}Al_{0.05}Mg_{0.025}Fe_{0.025}O_2$ materials.

The powder XRD diffractograms of all four materials gave sharp peaks due to good crystallinity. All the samples have similar reflection peaks at similar angles, indicating that all the materials are isostructural with $LiNi_{0.8}Co_{0.2}O_2$ and, therefore, can be indexed in the R3m space group [7]. $\left(\frac{I_{003}}{I_{104}}\right)$ intensity ratio plays a part in showing the characterization of an ordered or disordered lamellar phase. The $\left(\frac{I_{003}}{I_{104}}\right)$ ratio >1.0 is an indication of highly ordered lamellar phase with no cation mixing and vice versa [19]. All four samples gave different peak intensities. The relative intensity ratio of the $\left(\frac{I_{003}}{I_{104}}\right)$ peaks for (C1) $LiNi_{0.8}Co_{0.2}O_2$, (C2) $LiNi_{0.8}Co_{0.1}Al_{0.1}O_2$, and (C3) $LiNi_{0.8}Co_{0.1}Al_{0.05}Mg_{0.05}O_2$ is 1.3, 1.3, and 1.0, respectively, and show no cation mixing.

The (C4) $LiNi_{0.8}Co_{0.1}Al_{0.05}Mg_{0.025}Fe_{0.025}O_2$ has a ratio of 0.52 and shows cation mixing. When the $\left(\frac{I_{003}}{I_{104}}\right)$ ratio is more than 1.0 the nontransition metals like Al and Mg will occupy the Ni and Co sites only, whereas if the ratio is smaller than 1.0, the nontransition metals will occupy the lithium sites, too [20]. Chang et al. [21] have indicated that Mg^{2+} ions occupy only the Ni and Co sites in the structure of the $Li(Ni_{0.8}Co_{0.11}Mg_{0.09})O_2$ material, and Madhavi et al.

Table 1 Atomic ratios of elements in the materials and the amounts of chemicals used

Sample		Li	Ni	Co	Al	Mg	Fe
C_1	Amount used to synthesize (g)	68.95	232.65	56.20	–	–	–
	Atomic percent in EDAX	–	79.89	20.11	–	–	–
	Mole ratio of the metals	1.0	0.8	0.2	–	–	–
C_2	Amount used to synthesize (g)	68.95	232.65	28.11	37.51	–	–
	Atomic percent in EDAX	–	77.90	11.40	10.70	–	–
	Mole ratio of the metals	1.0	0.8	0.1	0.1	–	–
C_3	Amount used to synthesize (g)	68.95	232.65	28.11	18.76	12.82	–
	Atomic percent in EDAX	–	82.72	8.76	4.44	4.07	–
	Mole ratio of the metals	1.0	0.8	0.1	0.05	0.05	–
C_4	Amount used to synthesize (g)	68.95	232.65	28.11	18.76	6.41	10.1
	Atomic percent in EDAX	–	80.71	11.41	3.14	1.60	3.14
	Mole ratio of the metals	1.0	0.8	0.1	0.05	0.025	0.025

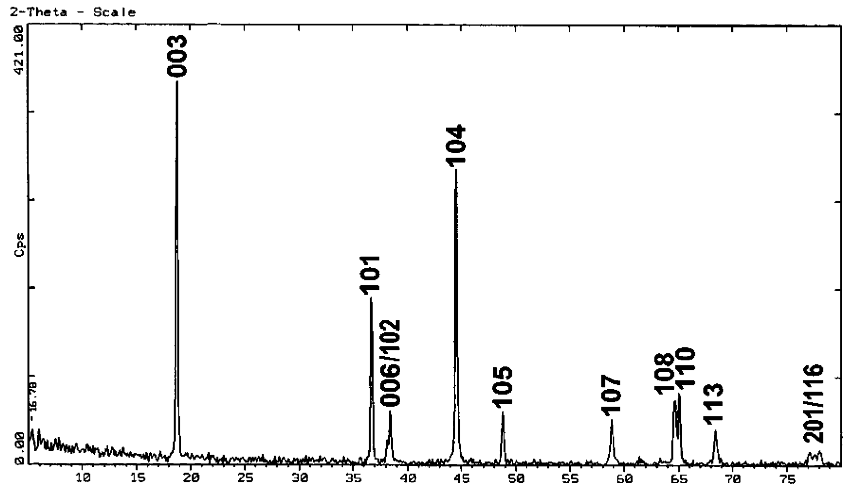

Fig. 1 Power XRD for (C1) $LiNi_{0.8}Co_{0.2}O_2$

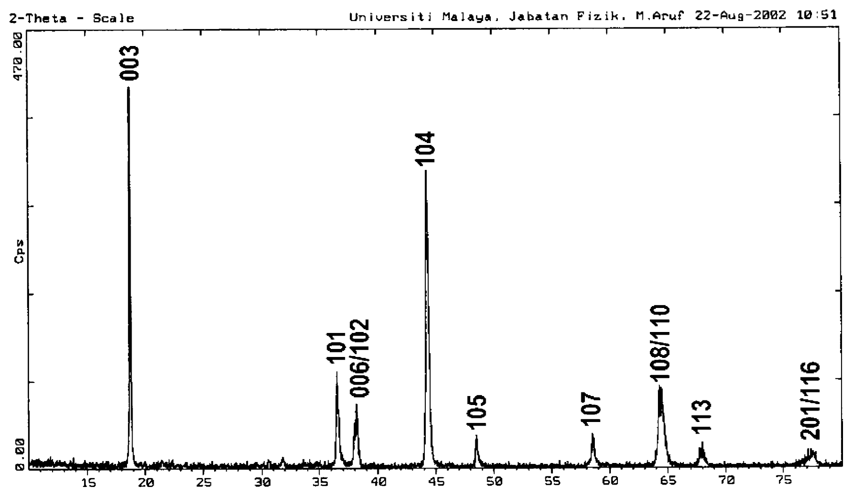

Fig. 2 Powder XRD for (C2) $LiNi_{0.8}Co_{0.1}Al_{0.1}O_2$

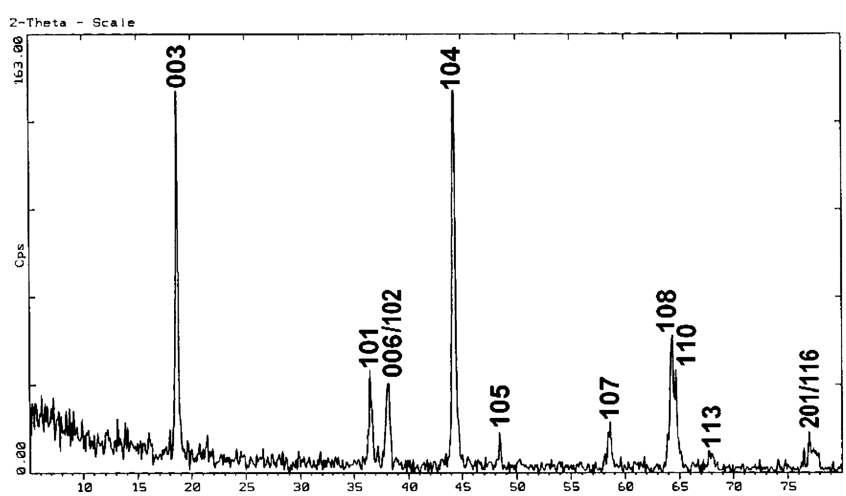

Fig. 3 Powder XRD for (C3) $LiNi_{0.8}Co_{0.1}Al_{0.05}Mg_{0.05}O_2$

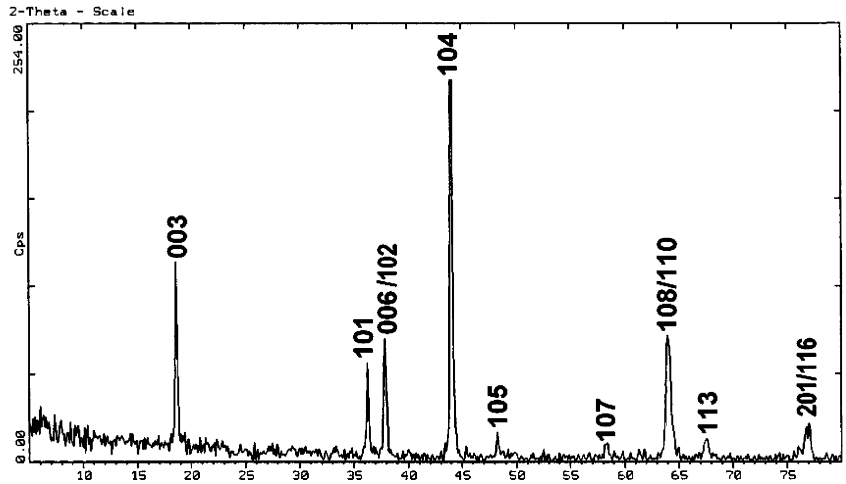

Fig. 4 Powder XRD for (C4) $LiNi_{0.8}Co_{0.1}Al_{0.05}Mg_{0.025}Fe_{0.025}O_2$

[9] have shown that Al^{3+} ions occupy only the Ni and Co sites in the $Li(Ni_{0.7}Co_{0.3-z}Al_z)O_2$ structure. Both materials have the intensity ratio $\left(\frac{I_{003}}{I_{104}}\right)$ of more than 1.0. It was also stated that with cation mixing in the materials, the Mg^{2+} or Ni^{2+} ions may occupy the lithium sites in the lattice [9].

For the (C4) $LiNi_{0.8}Co_{0.1}Al_{0.05}Mg_{0.025}Fe_{0.025}O_2$ material, based on the $\left(\frac{I_{003}}{I_{104}}\right)$ ratio, it can be concluded that there are some Mg^{2+} or Al^{3+} ions which occupy the lithium sites. The relative peak intensities of (006) and (101), $\left(\frac{I_{006}}{I_{101}}\right)$ for (C1) $LiNi_{0.8}Co_{0.2}O_2$, (C2) $LiNi_{0.8}Co_{0.1}Al_{0.1}O_2$, (C3) $LiNi_{0.8}Co_{0.1}Al_{0.05}Mg_{0.05}O_2$, and (C4) $LiNi_{0.8}Co_{0.1}Al_{0.05}Mg_{0.025}Fe_{0.025}O_2$ is 0.32, 0.64, 0.87, and 0.79, respectively. The splitting of the (006) and (102) peaks and the (108) and (110) peaks had occurred in the (C1) $LiNi_{0.8}Co_{0.2}O_2$ and (C2) $LiNi_{0.8}Co_{0.1}Al_{0.1}O_2$ materials, but the splitting is not clearly visible in (C3) $LiNi_{0.8}Co_{0.1}Al_{0.05}Mg_{0.05}O_2$ and (C4) $LiNi_{0.8}Co_{0.1}Al_{0.05}Mg_{0.025}Fe_{0.025}O_2$.

Electrochemical studies

Electrical conductivity and thermoelectrical power measurement evidenced a gradual change in the electronic properties from electron localization to electron delocalization upon lithium deintercalation [22]. A strong increase in the conductivity and the transition from semiconductor behavior to metallic behavior were reported, as a consequence of the creation of holes in the t_2 band upon lithium deintercalation [22]. According to Menestrier and colleagues [24], the metal–nonmetal transition was the driving force for the existence of the biphasic domain, in agreement with the experimental results of Imanishi et al. [23]. Pseudometallic behavior is observed, as conductivity increases with decreasing temperature [22].

Impedance spectroscopy was done on all four materials. Figure 5 shows the Nyquist plots taken at different temperatures for the (C1) $LiNi_{0.8}Co_{0.2}O_2$ material. It gave

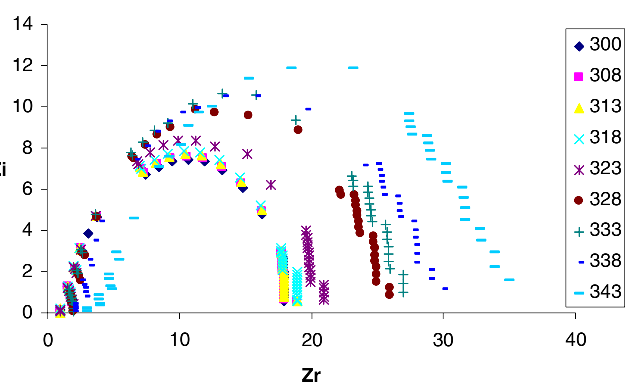

Fig. 5 Nyquist plots taken at different temperatures for the (C1) $LiNi_{0.8}Co_{0.2}O_2$ material

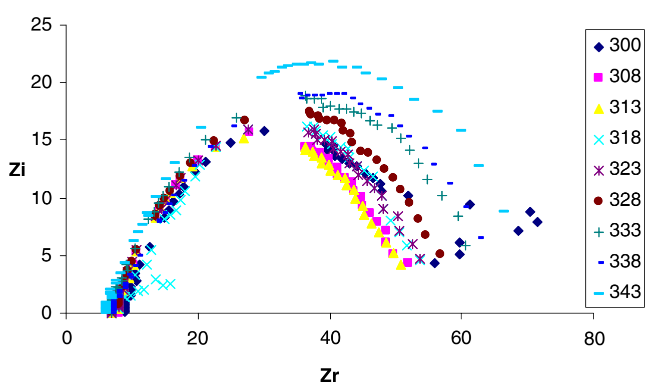

Fig. 6 Nyquist plots taken at different temperatures for the (C2) $LiNi_{0.8}Co_{0.1}Al_{0.1}O_2$ material

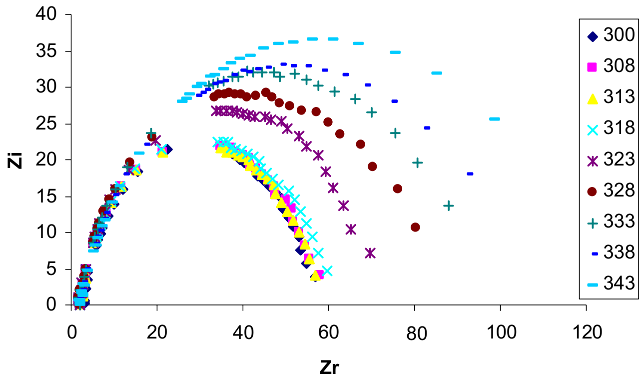

Fig. 7 Nyquist plots taken at different temperatures for the (C3) $LiNi_{0.8}Co_{0.1}Al_{0.05}Mg_{0.05}O_2$ material

a conductivity of 1.18×10^{-3} S cm^{-1} for the lowest temperature of 300 K and conductivity decreases with increasing temperature. Nyquist plots of the (C2) $LiNi_{0.8}Co_{0.1}Al_{0.1}O_2$, (C3) $LiNi_{0.8}Co_{0.1}Al_{0.05}Mg_{0.05}O_2$, and (C4) $LiNi_{0.8}Co_{0.1}Al_{0.05}Mg_{0.025}Fe_{0.025}O_2$ materials were obtained at different temperatures and are shown in Figs. 6, 7, and 8, respectively. The conductivity at 300 K for the (C2) $LiNi_{0.8}Co_{0.1}Al_{0.1}O_2$ and (C3) $LiNi_{0.8}Co_{0.1}Al_{0.05}Mg_{0.05}O_2$ material is 5.0×10^{-4} and 3.51×10^{-4} S cm^{-1}, respectively.

The (C4) $LiNi_{0.8}Co_{0.1}Al_{0.05}Mg_{0.025}Fe_{0.025}O_2$ material exhibits the lowest conductivity of 3.03×10^{-4} S cm^{-1} for all temperatures. Variations of the logarithm of the electrical conductivity (S cm^{-1}) vs. reciprocal temperature (K^{-1}) of all four materials are shown in Fig. 9. Figure 10 shows the comparisons in electrical conductivities at each temperature to examine the differences in each material. Table 2 gives the activation energy of the materials from the conductivity measurement calculated from the Arrhenius equation:

$$\ln k = \ln A - \frac{E_A}{RT}$$

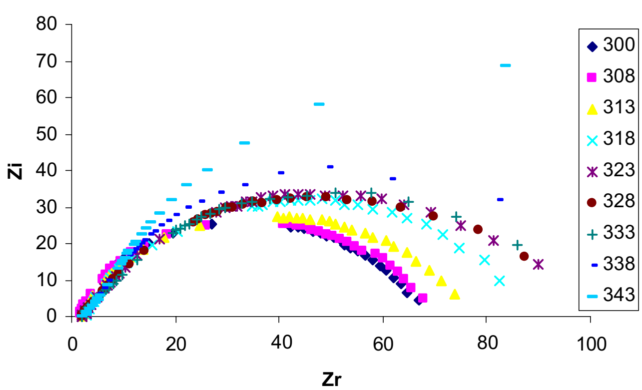

Fig. 8 Nyquist plots taken at different temperatures for the (C4) $LiNi_{0.8}Co_{0.1}Al_{0.05}Mg_{0.025}Fe_{0.025}O_2$ material

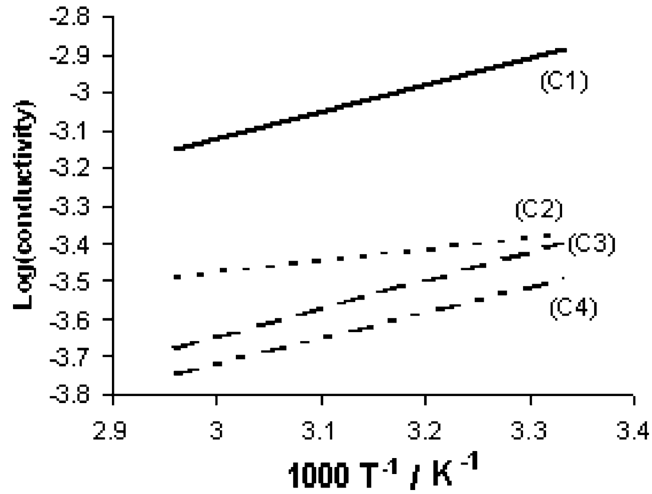

Fig. 9 Log (k/S cm^{-1}) vs. the reciprocal of temperature 1,000 T^{-1}/K^{-1}

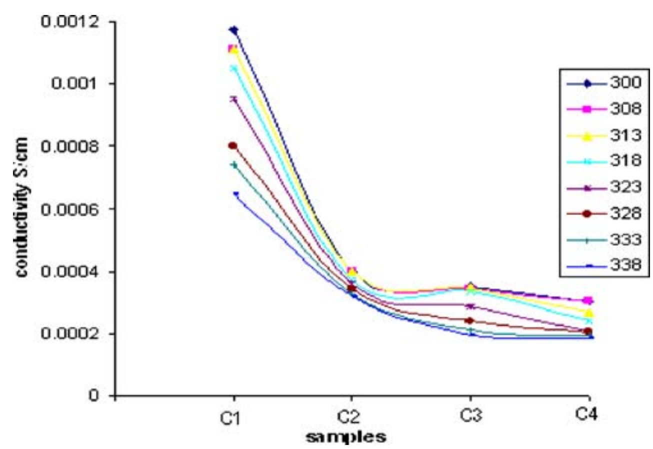

Fig. 10 The variation of conductivity k/S cm^{-1} with temperature for each sample

Table 2 Activation energies for all four cathodic materials

Sample	Material	E_a/kJ mol^{-1}
C1	$LiNi_{0.8}Co_{0.2}O_2$	−0.788
C2	$LiNi_{0.8}Co_{0.1}Al_{0.1}O_2$	−0.328
C3	$LiNi_{0.8}Co_{0.1}Al_{0.05}Mg_{0.05}O_2$	−0.841
C4	$LiNi_{0.8}Co_{0.1}Al_{0.05}Mg_{0.025}Fe_{0.025}O_2$	−0.667

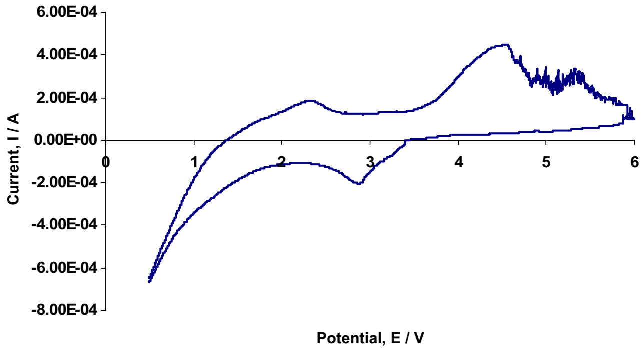

Fig. 11 Cyclic voltammogram for the (C1) $LiNi_{0.8}Co_{0.2}O_2$ material at 1×10^{-4} V s^{-1}

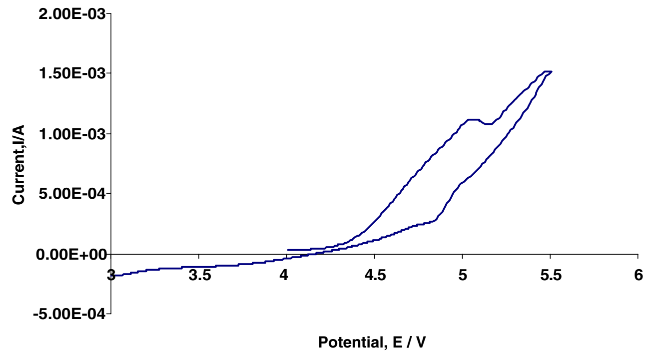

Fig. 13 Cyclic voltammogram for the (C3) $LiNi_{0.8}Co_{0.1}Al_{0.05}Mg_{0.05}O_2$ material at 1×10^{-4} V s^{-1}

From Fig. 10, the highest conductivity obtained was for (C1) $LiNi_{0.8}Co_{0.2}O_2$ for all temperatures and also showed larger variation of conductivity with temperature. With the introduction of nontransition metals such as Al and Mg, the conductivities of the materials decreased for each temperature and showed smaller variations with temperatures.

The conductivity and temperature variation studies suggest that the materials experience phase transformation from semiconductor to pseudometallic phase, as also been suggested by other workers [22] because metal conductivity also decrease with temperature increase.

Cyclic voltammetry was done to examine the oxidation–reduction peaks of the materials. The oxidation peak had occurred at about 4.5 V and the reduction peak at 2.9 V while a smaller oxidation peak can be seen at 2.3 V for the 0.1 mV s^{-1} scan rate for the (C1) $LiNi_{0.8}Co_{0.2}O_2$ material shown in Fig. 11.

Figure 12 shows the voltammogram for the (C2) $LiNi_{0.8}Co_{0.1}Al_{0.1}O_2$ material at 1×10^{-4} V s^{-1} scan rate and have one oxidation–reduction pair of peaks at around 2.4 and 2.6 V, respectively.

The voltammograms for the (C3) $LiNi_{0.8}Co_{0.1}Al_{0.05}Mg_{0.05}O_2$ and (C4) $LiNi_{0.8}Co_{0.1}Al_{0.05}Mg_{0.025}Fe_{0.025}O_2$ materials are shown in Figs. 13 and 14, respectively. From Fig. 13, the cyclic voltammogram at 1×10^{-4} V s^{-1} for (C3) $LiNi_{0.8}Co_{0.1}Al_{0.05}Mg_{0.05}O_2$ gave oxidation–reduction peaks at 5.0 and 4.8 V, respectively. While in Fig. 14, the cyclic voltammogram at 1×10^{-4} V s^{-1} for (C4) $LiNi_{0.8}Co_{0.1}Al_{0.05}Mg_{0.025}Fe_{0.025}O_2$ gave oxidation–reduction peaks at 6.5 and 6.0 V, respectively.

Conclusion

The (C1) $LiNi_{0.8}Co_{0.2}O_2$, (C2) $LiNi_{0.8}Co_{0.1}Al_{0.1}O_2$, (C3) $LiNi_{0.8}Co_{0.1}Al_{0.05}Mg_{0.05}O_2$, and (C4) $LiNi_{0.8}Co_{0.1}Al_{0.05}Mg_{0.025}Fe_{0.025}O_2$ cathode materials were synthesized via solid-state method at a temperature of 800 °C for 18 h. Powder XRD of all four materials showed crystalline phase and isostructural with the (C1) $LiNi_{0.8}Co_{0.2}O_2$ material. Impedance spectroscopy studies gave highest conductivity for the (C1) $LiNi_{0.8}Co_{0.2}O_2$ material at all temperatures, and all four materials have decreasing conductivities with increasing temperatures. The addition of nontransition metals such as Al and Mg actually decreased the conductivities at all temperatures.

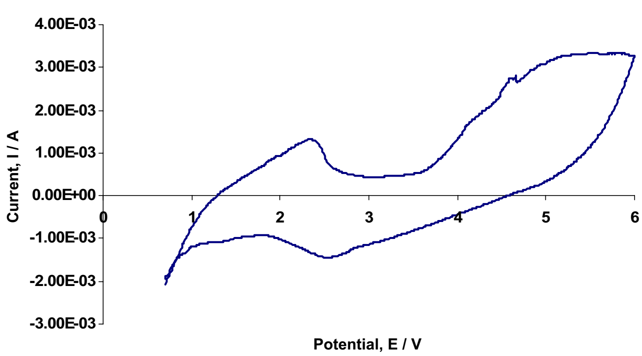

Fig. 12 Cyclic voltammogram for the (C2) $LiNi_{0.8}Co_{0.1}Al_{0.1}O_2$ material at 1×10^{-4} V s^{-1}

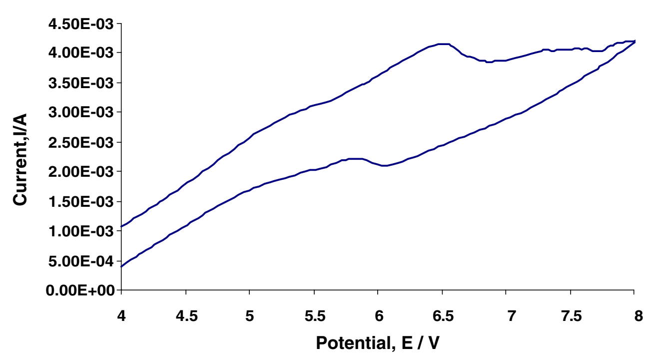

Fig. 14 Cyclic voltammogram for the (C4) $LiNi_{0.8}Co_{0.1}Al_{0.05}Mg_{0.025}Fe_{0.025}O_2$ material at 1×10^{-4} V s^{-1}

References

1. Dahn JR, von Sacken U, Michal CA (1990) Solid State Ionics 44:87–97
2. Ohzuku T, Ueda A, Nagayama M (1993) J Electrochem Soc 140:1862–1870
3. Brousseley M, Planchat JP, Rigobert G, Virey D, Sarre G (1997) J Power Sources 68:8–12
4. Ohzuku T, Ueda A (1994) Solid State Ionics 69:201–211
5. Dahn JR, Sacken UV, Juzkow MW, Al-Anaby H (1991) J Electrochem Soc 138:2207–2211
6. Broussely M, Perton F, Labat J, Staniewicz RJ, Romero A (1993) J Power Sources 43–44:209–216
7. Saadoune I, Delmas C (1998) J Solid State Chem 136:8–15
8. Fujita Y, Amine K, Maruta J, Yasuda H (2000) J Power Sources 90:82–88
9. Madhavi S, Subba Rao GV, Chowdari BVR, Li SFY (2002) Solid State Ionics 152–153:199–205
10. Guilmard M, Pouillerie C, Croguennec L, Delmas C (2003) Solid State Ionics 160:39–50
11. Delmas C, Saadoune I (1992) Solid State Ionics 53–56:370–375
12. Delmas C, Saadoune I, Rougier A (1993) J Power Sources 4344:595–602
13. Zhecheva E, Stoyanova R (1993) Solid State Ionics 66:143–149
14. Ueda A, Ohzuku T (1994) J Electrochem Soc 141(8):2010–2014
15. Rougier A, Saadoune I, Gravereau P, Willmann P, Delmas C (1996) Solid State Ionics 90:83–90
16. Madhavi S, Subba Rao GV, Chowdari BVR, Li SFY (2001) J Power Sources 93:156–162
17. Lee KK, Yoon WS, Kim KB, Lee KY, Hong ST (2001) J Power Sources 97–98:308–312
18. Weaving JS, Cowar F, Teagle DA, Cullen J, Dass V, Bindin P, Green R, Macklin WJ (2001) J Power Sources 97–98:733–735
19. Dahn JR, Von Sacken V, Micheal CA (1990) Solid State Ionics 44:87–97
20. Ooms FGB, Kelder EM, Schoonman J, Wagemaker M, Mulder FM (2002) Solid State Ionics 152–153:143–153
21. Chang CC, Kim JY, Kumta PN (2000) J Power Sources 89:56–63
22. Antolini E (2004) Solid State Ionics 170:159–171
23. Imanishi N, Fujiyoshi M, Takeda Y, Yamamoto O, Tabuchi T (1999) Solid State Ionics 118:121–128
24. Levasseur S, Menetrier M, Suard E, Delmas C (2000) Solid State Ionics 128:11–24